Acknowledgment. We thank Dr. Jeffrey R. Bocarsly for helpful discussions. We thank Dr. G. Papaefthymiou for help with the SQUID measurements. We thank the National Institutes of Health for support of this research through Grants GM-32715 and GM-40974 and the NSF for support (J.E.S.).

Supplementary Material Available: Tables listing temperature dependence, positional parameters, intramolecular distances and bond angles, torsion or conformation angles, and U values (19 pages); observed and calculated structure factors (26 pages). Ordering information is given on any current masthead page.

Spin Pairing and Magnetic Coupling in Quasi One-Dimensional Semiconductors with a Trimeric Stacking Structure. Structural, Charge-Transport, and Magnetic Studies of $[Ni(tatbp)]_3[ReO_4]_2 \cdot C_{10}H_7Cl$ and $[Cu(tatbp)]_3[ReO_4]_2 \cdot C_{10}H_7Cl$

Martin R. Godfrey, Timothy P. Newcomb, Brian M. Hoffman,* and James A. Ibers*

Contribution from the Department of Chemistry and Materials Research Center, Northwestern University, Evanston, Illinois 60208. *Received January 8, 1990*

Abstract: Electrochemical oxidation of (triazatetrabenzoporphyrinato)nickel(II) or (triazatetrabenzoporphyrinato)copper(II), Ni(tatbp) or Cu(tatbp), dissolved in 1-chloronaphthalene in the presence of the perrhenate ion affords the new molecular conductors $[Ni(tatbp)]_3[ReO_4]_2 \cdot C_{10}H_7Cl$ and $[Cu(tatbp)]_3[ReO_4]_2 \cdot C_{10}H_7Cl$. The isostructural compounds are composed of partially ligand-oxidized (+2/3) M(tatbp) molecules that form trimerized stacks. Trimerization of the conducting stacks renders the compounds semiconductors with conductivity along the needle axis (crystallographic a) in the range of 2.5×10^{-4}–3.0×10^{-4} Ω^{-1} cm^{-1} and an activation energy for conduction in the range of 0.24–0.26 eV. Magnetic susceptibility measurements on the Ni(II) derivative show that the valence band has the diamagnetic ground state expected for a semiconductor. Nonetheless, the valence-band electrons are shown to mediate a strong intratrimer Cu–Cu coupling characterized by a Weiss constant $\theta = -5.2$ K in the Cu(II) analogue. The magnetic properties are rationalized in terms of a band structure derived by considering the trimers as weakly interacting supermolecules, with θ dominated by intratrimer interactions. A structure determination was performed on the Cu(II) analogue. It crystallizes in space group C_i^1–$P\bar{1}$ of the triclinic system with one formula unit in a cell of dimensions $a = 9.167$ (6) Å, $b = 15.849$ (10) Å, $c = 16.065$ (10) Å, $\alpha = 65.87$ (2)°, $\beta = 72.11$ (3)°, and $\gamma = 84.01$ (2)° (volume = 2126 Å^3) at 110 K. The Cu–Cu distance for adjacent macrocycles within a trimer is 3.190 (3) Å and that between trimers is 3.482 (4) Å. The ReO_4^- anions lie within channels formed between the stacks as does a disordered 1-chloronaphthalene solvent molecule. The final refinement of 4988 observations having $F_o^2 > 3\sigma(F_o^2)$ involved an anisotropic model for Cu and Re, an isotropic model for the other non-hydrogen atoms, and fixed positions for the hydrogen atoms (295 variables). The refinement converged to values of $R(F) = 0.085$ and $R_w(F) = 0.091$.

Introduction

We have described a series of molecular conductors prepared by chemical oxidation of metalloporphyrins with molecular iodine.[1-7] These compounds are comprised of metal-over-metal stacks of partially oxidized (+1/3) metallomacrocycles (M(L)) surrounded by chains of I_3^- anions.[8,9] When oxidation occurs from the ligand-based p-π orbitals the result often is a highly conductive molecular metal. For example, crystals of Ni(pc)I (pc = phthalocyaninato), Cu(pc)I, and Cu(tatbp)I (tatbp = triazatetrabenzoporphyrinato) have room temperature conductivities of up to 750 Ω^{-1} cm^{-1} and Ni(pc)I has been shown to retain a metallic band structure even at very low temperatures.[1]

In the compounds Cu(pc)I and Cu(tatbp)I the carrier electrons in the ligand-based p-π conduction band interact with the magnetic

(1) (a) Schramm, C. J.; Scaringe, R. P.; Stojakovic, D. R.; Hoffman, B. M.; Ibers, J. A. *J. Am. Chem. Soc.* **1980**, *102*, 6702–6713. (b) Martinsen, J.; Greene, R. L.; Palmer, S. M.; Hoffman, B. M.; Ibers, J. A. *J. Am. Chem. Soc.* **1983**, *105*, 677–678. (c) Martinsen, J.; Palmer, S. M.; Tanaka, J.; Greene, R. L.; Hoffman, B. M. *Phys. Rev. B* **1984**, *30*, 6269–6276.

(2) Martinsen, J.; Pace, L. J.; Phillips, T. E.; Hoffman, B. M.; Ibers, J. A. *J. Am. Chem. Soc.* **1982**, *104*, 83–91.

(3) Pace, L. J.; Martinsen, J.; Ulman, A.; Hoffman, B. M.; Ibers, J. A. *J. Am. Chem. Soc.* **1983**, *105*, 2612–2620.

(4) Martinsen, J.; Stanton, J. L.; Greene, R. L.; Tanaka, J.; Hoffman, B. M.; Ibers, J. A. *J. Am. Chem. Soc.* **1985**, *107*, 6915–6920.

(5) Hoffman, B. M.; Ibers, J. A. *Acc. Chem. Res.* **1983**, *16*, 15–21.

(6) (a) Ogawa, M. Y.; Martinsen, J.; Palmer, S. M.; Stanton, J. L.; Tanaka, J.; Greene, R. L.; Hoffman, B. M.; Ibers, J. A. *J. Am. Chem. Soc.* **1987**, *109*, 1115–1121. (b) Ogawa, M. Y.; Hoffman, B. M.; Lee, S.; Yadkowsky, M.; Halperin, W. P. *Phys. Rev. Lett.* **1986**, *57*, 1177–1180.

(7) (a) Liou, K. K.; Ogawa, M. Y.; Newcomb, T. P.; Quirion, G.; Lee, M.; Poirier, M.; Halperin, W. P.; Hoffman, B. M.; Ibers, J. A. *Inorg. Chem.* **1989**, *28*, 3889–3896. (b) Quirion, G.; Poirier, M.; Ogawa, M. Y.; Hoffman, B. M. *Solid State Commun.* **1987**, *64*, 613–616. (c) Quirion, G.; Poirier, M.; Liou, K. K.; Ogawa, M. Y.; Hoffman, B. M. *Phys. Rev. B* **1988**, *37*, 4272–4275. (d) Ogawa, M. Y.; Palmer, S. M.; Liou, K. K.; Quirion, G.; Thompson, J. A.; Poirier, M.; Hoffman, B. M. *Phys. Rev. B* **1989**, *39*, 10682–10692.

(8) Similar structures are produced by electrochemical oxidation of metallomacrocycles. (a) Yakushi, K.; Yamakado, H.; Yoshitake, M.; Kosugi, N.; Kuroda, H.; Sugano, T.; Kinoshita, M.; Kawamoto, A.; Tanaka, J. *Bull. Chem. Soc. Jpn.* **1989**, *69*, 687–696. (b) Yakushi, K.; Yamakado, H.; Yoshitake, M.; Kosugi, N.; Kuroda, H.; Kowamoto, A.; Tanaka, J.; Sugano, T.; Kinoshita, M.; Hino, S. *Synth. Met.*, **1989**, *29*, F95–F102. (c) Almeida, M.; Kanatzidis, M. G.; Tonge, L. M.; Marks, T. J.; Marcy, H. O.; McCarthy, W. J.; Kannewurf, C. R. *Solid State Commun.* **1987**, *63*, 457–461. (d) Newcomb, T. P.; Godfrey, M. R.; Hoffman, B. M.; Ibers, J. A. *J. Am. Chem. Soc.* **1989**, *111*, 7078–7084.

(9) Other structural types have been prepared with M(pc) systems of higher coordination number. For example see: (a) Wynne, K. J. *Inorg. Chem.* **1985**, *24*, 1339–1343. (b) Hanack, M. *Mol. Cryst. Liq. Cryst.* **1988**, *160*, 133–137. (c) Mossoyan-Deneux, M.; Benlian, D.; Baldy, A.; Pierrot, M. *Mol. Cryst. Liq. Cryst.* **1988**, *156*, 247–256. (d) Mossoyan-Deneux, M.; Benlian, D.; Pierrot, M.; Fournel, A.; Sobier, J. P. *Inorg. Chem.* **1985**, *24*, 1878–1882. (e) Pietro, W. J.; Marks, T. J.; Ratner, M. A. *J. Am. Chem. Soc.* **1985**, *107*, 5387–5391.

0002-7863/90/1512-7260$02.50/0 © 1990 American Chemical Society

copper(II) ions (d^9, $S = {}^1/_2$) at the center of each macrocycle.[6,7] Strong intramolecular spin exchange between the mobile carriers and the localized Cu(II) moments leads to carrier-mediated long-range Cu–Cu coupling along the one-dimensional chains of Cu(II) ions and gives rise to novel magnetic phenomena at low temperatures.

We have prepared two compounds $[M(tatbp)]_3[ReO_4]_2 \cdot C_{10}H_7Cl$ (M = Ni, Cu) that are semiconductors because of an increased degree of partial oxidation (+2/3) and a structure that is comprised of stacks of $[M(L)]_3^{2+}$ trimers. Previous magnetic resonance studies performed by other investigators on partially oxidized solutions of metalloporhyrins point to the formation of trimeric aggregates similar to those observed here in the solid state.[10] Such solution aggregates have paired π-electrons. Similarly, the properties of the present semiconductors can be rationalized by viewing their structures as weakly interacting stacks of spin-paired supermolecules.

Even though the carrier concentration in these materials is negligible, electrons in the p-π bands of the Cu compound nonetheless mediate strong intrastack spin exchange. Measurements on a solid solution $[Ni_{1-x}Cu_x(tatbp)]_3[ReO_4]_2 \cdot C_{10}H_7Cl$ suggest that the Cu–Cu coupling is mainly associated with π-electron delocalization within trimers and thus the range of this interaction is greatly reduced from that observed in the molecular metals prepared by iodine oxidation of the Cu(L).

Experimental Section

Preparation of Ni(tatbp) and Cu(tatbp). (Triazatetrabenzoporphyrinato)magnesium (Mg(tatbp)) was prepared according to the literature synthesis.[11] The crude product was demetalated by dissolution in concentrated sulfuric acid and purified by filtration through sand onto a mixture of NH_4OH and ice. The free base triazatetrabenzoporphyrin (H_2(tatbp)) was separated from the aqueous phase by filtration and the resultant material was sublimed under vacuum prior to further use. Nickel(II) and copper(II) derivatives were prepared by stirring H_2(tatbp) in 1-chloronaphthalene at 180 °C or above for several hours with an excess of the metal chloride. The progress of the metalation reaction was monitored by optical spectroscopy. When metalation was complete the product was isolated by filtration and vacuum sublimed at least twice before further use.

Preparation of $[Ni(tatbp)]_3[ReO_4]_2 \cdot C_{10}H_7Cl$ and $[Cu(tatbp)]_3[ReO_4]_2 \cdot C_{10}H_7Cl$. Single crystals of $[Ni(tatbp)]_3[ReO_4]_2 \cdot C_{10}H_7Cl$ or $[Cu(tatbp)]_3[ReO_4]_2 \cdot C_{10}H_7Cl$ were grown at the anode of an electrolytic cell that consisted of two compartments separated by a medium porosity frit. The cells were suspended in a stirred oil bath. The temperature of the bath was controlled at 150 °C to a precision of ±1 °C. A 2.0×10^{-2} M solution of $[N(n\text{-}Bu)_4][ReO_4]$ in freshly vacuum distilled 1-chloronaphthalene was saturated in M(tatbp) by stirring with an excess of solid M(tatbp) at 150 °C overnight. The resulting solution was then filtered and placed while still hot in both compartments of the thermostated electrolytic cell. Platinum electrodes were immersed in both compartments and a constant current of 5.0 μA was passed through the cell for 2 weeks. Crystals of $[Ni(tatbp)]_3[ReO_4]_2 \cdot C_{10}H_7Cl$ or $[Cu(tatbp)]_3[ReO_4]_2 \cdot C_{10}H_7Cl$ that are needle-shaped and hexagonal in cross section were harvested from the anode surface. Elemental analyses, carried out by Micro-Tech Laboratories Inc. (Skokie, IL) are consistent with the formulas $[Ni(tatbp)]_3[ReO_4]_2 \cdot C_{10}H_7Cl$ and $[Cu(tatbp)]_3[ReO_4]_2 \cdot C_{10}H_7Cl$. Anal. Calcd for $C_{109}H_{58}ClCu_3N_{21}O_8Re_2$: C, 54.82; H, 2.45; N, 12.32. Found: C, 55.17; H, 2.41; N, 11.76. Calcd for $C_{109}H_{58}ClNi_3N_{21}O_8Re_2$: C, 54.93; H, 2.45; N, 12.34. Found: C, 55.08; H, 2.39; N, 11.72.

Preparation of $[Ni_{1-x}Cu_x(tatbp)]_3[ReO_4]_2 \cdot C_{10}H_7Cl$. A $[Ni_{1-x}Cu_x(tatbp)]_3[ReO_4]_2 \cdot C_{10}H_7Cl$ solid solution was prepared by electrocrystallization as above but with the use of a solution of one part Cu(tatbp) to six parts Ni(tatbp) in 1-chloronaphthalene. The composition of the "alloy" was determined by measuring the Curie constant of the material and comparing it to the Curie constant expected for $[Cu(tatbp)]_3[ReO_4]_2 \cdot C_{10}H_7Cl$, with the result that $x = 0.28$. This technique was developed and discussed in ref 7d.

X-ray Diffraction Study of $[Cu(tatbp)]_3[ReO_4]_2 \cdot C_{10}H_7Cl$. From precession and Weissenberg photography crystals of $[M(tatbp)]_3[ReO_4]_2 \cdot C_{10}H_7Cl$ (M = Cu, Ni) are isostructural and belong to the triclinic system. Cell constants for M = Cu were determined from the setting angles of 25 reflections that had been centered on a Picker FACS-1 diffractometer. These and other details of the data collection are given in Table I. Intensity data were collected by methods standard in this laboratory.[12]

Table I. Crystal Data and Experimental Details for $[Cu(tatbp)]_3[ReO_4]_2 \cdot C_{10}H_7Cl$

compd	tris(triazatetrabenzoporphyrinato)copper(II) diperrhenate 1-chloronaphthalene solvate
formula	$C_{109}H_{58}ClCu_3N_{21}O_8Re_2$
formula wt, amu	2388.2
a, Å	9.167 (6)
b, Å	15.849 (10)
c, Å	16.065 (10)
α, deg	65.87 (2)
β, deg	72.11 (3)
γ, deg	84.01 (2)
V, Å^3	2126
temp, K	110[a]
Z	1
d_{calc}, g/cm^3	1.865
space group	C_i^1–$P\bar{1}$
crystal shape	needle of hexagonal cross section, 0.5 mm in length, 0.15 mm across with needle axis a
crystal vol, mm^3	0.0062
radiation	Mo Kα (λMo Kα_1 = 0.70930 Å)
μ, cm^{-1}	37.24
transmission factors[b]	0.61 to 0.74
receiving aperture	5 mm vertical by 4 mm horizontal 32 cm from crystal
scan speed, deg/min	2.0 in 2θ
scan method	θ–2θ
background counts	20 s at each end of scan with rescan option[c]
scan range	−1.0 to 1.0 in 2θ
collection limits	$2 \le 2\theta \le 50°$
data collected	$\pm h \pm k \pm l$
p factor	0.04
no. of data collected	7449
no. of unique data having $F_o^2 > 3\sigma(F_o^2)$	4998
no. of variables	295
R on F	0.085
R_w on F	0.091
error in obsd unit wt	2.20

[a] The low-temperature system based on a design by: Huffman, J. C. Ph.D. Thesis, Indiana University, 1974. [b] The analytical absorption correction was performed with the use of the Northwestern absorption program AGNOST. See: de Meulenaer, J.; Tompa, H. *Acta Crystallogr.* **1965**, *19*, 1014–1018. [c] The Picker FACS-1 diffractometer was operated under the Vanderbilt disk-oriented system: Lenhert, P. G. *J. Appl. Crystallogr.* **1975**, *8*, 568.

The structure was solved through use of the program SHEL86.[13] In the final model anisotropic thermal parameters were assigned to the metal atoms and isotropic thermal parameters to the remaining non-hydrogen atoms. Hydrogen atoms were fixed by geometry (C–H = 0.95 Å) and were not varied. The tatbp unit was assumed to be 4-fold disordered so that atoms N(2), N(4), N(6), and N(8) were taken to be 75% N and 25% C with the scattering factor adjusted accordingly. Because the 1-chloronaphthalene solvate lies very close to a center of symmetry and is disordered, the $C_{10}H_7$ portion of that molecule was refined as a rigid group,[14] while the Cl atom was varied independently. The relatively high agreement indices of Table I result from difficulties with solvent disorder. Final positional and equivalent isotropic thermal parameters are given in Table II. Table III[15] presents the anisotropic thermal parameters for Cu and Re. Table IV[15] provides a listing of $10|F_o|$ vs $10|F_c|$.

Electron Spin Resonance Measurements. Powder and single crystal electron spin resonance (ESR) spectra were obtained on a modified Varian E-4 X-band spectrometer or a Varian E-109 Q-band spectrometer

(10) Godziela, G. M.; Goff, H. M. *J. Am. Chem. Soc.* **1986**, *108*, 2237–2243.
(11) Barrett, P. A.; Linstead, R. P.; Tuey, G. A. P.; Robertson, J. M. *J. Chem. Soc.* **1939**, 1809–1820.
(12) Corfield, P. W. R.; Doedens, R. J.; Ibers, J. A. *Inorg. Chem.* **1967**, *6*, 197–204.
(13) Sheldrick, G. M. In *Crystallographic Computing 3*; Sheldrick, G. M., Kruger, C., Goddard, R., Eds.; Oxford University Press: London, 1985; pp 175–189.
(14) La Placa, S. J.; Ibers, J. A. *Acta Crystallogr.* **1965**, *18*, 511–519.
(15) Supplementary material.

Table II. Positional Parameters and B_{eq} (Å^2) Values for $[Cu(tatbp)]_3[ReO_4]_2 \cdot C_{10}H_7Cl$

atom	x	y	z	B	atom	x	y	z	B
Re	0.18549 (10)	0.83629 (05)	0.30664 (05)	3.83 (3)	C(8)2	0.0233 (14)	0.2955 (08)	0.1022 (08)	1.3 (2)
Cu(1)	0.33081 (17)	0.53578 (09)	−0.01891 (10)	1.13 (5)	C(9)2	0.0796 (14)	0.3450 (08)	−0.0634 (08)	1.3 (2)
Cu(2)	0	1/2	0	1.01 (7)	C(10)2	0.1269 (15)	0.3250 (08)	−0.1484 (09)	1.4 (2)
Cl	0.2737 (10)	0.1026 (05)	−0.3963 (06)	3.3 (2)	C(11)2	0.1627 (15)	0.2430 (08)	−0.1613 (08)	1.5 (2)
N(1)1	0.3777 (11)	0.5769 (06)	−0.1574 (07)	1.1 (2)	C(12)2	0.2076 (16)	0.2496 (09)	−0.2548 (09)	1.9 (2)
N(2)1	0.4330 (12)	0.4300 (07)	−0.1733 (07)	1.3 (2)	C(13)2	0.2134 (16)	0.3339 (09)	−0.3318 (09)	1.9 (2)
N(3)1	0.3690 (11)	0.4078 (06)	−0.0071 (07)	1.1 (2)	C(14)2	0.1742 (15)	0.4148 (08)	−0.3179 (09)	1.6 (2)
N(4)1	0.3152 (12)	0.3273 (07)	0.1642 (07)	1.2 (2)	C(15)2	0.1355 (14)	0.4097 (08)	−0.2261 (08)	1.3 (2)
N(5)1	0.2824 (12)	0.4921 (07)	0.1205 (07)	1.2 (2)	C(16)2	0.0914 (14)	0.4781 (08)	−0.1851 (08)	1.2 (2)
N(6)1	0.2205 (14)	0.6398 (08)	0.1369 (08)	2.0 (2)	H031	0.3956	0.8006	−0.4099	2.5
N(7)1	0.2882 (11)	0.6631 (07)	−0.0307 (07)	1.1 (2)	H041	0.4324	0.7608	−0.5423	3.4
N(8)1	0.3377 (12)	0.7415 (07)	−0.2034 (07)	1.4 (2)	H051	0.4877	0.6070	−0.5269	2.8
C(1)1	0.3733 (15)	0.6661 (08)	−0.2218 (09)	1.4 (2)	H061	0.4898	0.4905	−0.3800	2.4
C(2)1	0.4098 (14)	0.6678 (08)	−0.3179 (08)	1.4 (2)	H111	0.4820	0.2385	−0.1566	2.9
C(3)1	0.4113 (15)	0.7384 (08)	−0.4042 (09)	1.6 (2)	H121	0.4563	0.0770	−0.0532	3.2
C(4)1	0.4374 (17)	0.7142 (10)	−0.4818 (10)	2.3 (3)	H131	0.4130	0.0271	0.1087	3.2
C(5)1	0.4665 (16)	0.6229 (09)	−0.4727 (10)	2.1 (2)	H141	0.3575	0.1352	0.1819	2.7
C(6)1	0.4669 (16)	0.5532 (09)	−0.3866 (09)	1.9 (2)	H191	0.2313	0.2610	0.3694	2.5
C(7)1	0.4370 (15)	0.5783 (08)	−0.3090 (09)	1.6 (2)	H201	0.1406	0.2877	0.5100	2.7
C(8)1	0.4165 (15)	0.5221 (08)	−0.2083 (09)	1.5 (2)	H211	0.0949	0.4414	0.4987	2.9
C(9)1	0.4084 (15)	0.3784 (08)	−0.0812 (09)	1.5 (2)	H221	0.1417	0.5682	0.3507	2.4
C(10)1	0.4218 (15)	0.2771 (08)	−0.0429 (08)	1.4 (2)	H271	0.1591	0.8360	0.1152	2.2
C(11)1	0.4536 (16)	0.2173 (09)	−0.0870 (09)	2.0 (2)	H281	0.1450	0.9939	0.0140	2.8
C(12)1	0.4438 (17)	0.1231 (10)	−0.0276 (10)	2.4 (3)	H291	0.1989	1.0396	−0.1496	3.3
C(13)1	0.4116 (17)	0.0928 (09)	0.0710 (10)	2.2 (3)	H301	0.2689	0.9328	−0.2217	2.9
C(14)1	0.3802 (16)	0.1554 (09)	0.1144 (09)	1.9 (2)	H032	−0.0799	0.2815	0.3525	2.4
C(15)1	0.3886 (15)	0.2487 (08)	0.0547 (09)	1.6 (2)	H042	−0.0617	0.0900	0.4568	2.8
C(16)1	0.3537 (14)	0.3308 (08)	0.0772 (08)	1.3 (2)	H052	0.0074	0.0158	0.3498	3.1
C(17)1	0.2794 (14)	0.4011 (08)	0.1850 (08)	1.3 (2)	H062	0.0527	0.0986	0.1876	2.4
C(18)1	0.2338 (15)	0.3966 (08)	0.2806 (09)	1.5 (2)	H112	0.1605	0.1854	−0.1101	2.4
C(19)1	0.2095 (15)	0.3220 (08)	0.3673 (09)	1.7 (2)	H122	0.2338	0.1955	−0.2663	2.8
C(20)1	0.1582 (15)	0.3403 (09)	0.4483 (09)	1.7 (2)	H132	0.2433	0.3334	−0.3939	2.7
C(21)1	0.1293 (16)	0.4303 (09)	0.4428 (09)	1.8 (2)	H142	0.1801	0.4736	−0.3723	2.5
C(22)1	0.1567 (15)	0.5055 (08)	0.3563 (09)	1.6 (2)	C(1)S	0.3580 (25)	0.0549 (20)	−0.4820 (21)	8. (2)
C(23)1	0.2062 (15)	0.4872 (08)	0.2740 (09)	1.4 (2)	C(2)S	0.3208 (27)	0.0435 (21)	−0.5560 (22)	3. (1)
C(24)1	0.2365 (14)	0.5452 (08)	0.1734 (08)	1.0 (2)	C(3)S	0.416 (03)	−0.0058 (21)	−0.6071 (18)	5. (1)
C(25)1	0.2442 (15)	0.6956 (08)	0.0405 (09)	1.5 (2)	C(4)S	0.546 (03)	−0.0428 (18)	−0.5833 (17)	8. (1)
C(26)1	0.2274 (14)	0.7906 (08)	0.0038 (08)	1.2 (2)	C(5)S	0.5809 (22)	−0.0304 (15)	−0.5089 (15)	4.7 (8)
C(27)1	0.1828 (15)	0.8561 (08)	0.0467 (09)	1.6 (2)	C(6)S	0.7121 (23)	−0.0682 (16)	−0.4866 (15)	7. (1)
C(28)1	0.1728 (16)	0.9476 (09)	−0.0125 (10)	2.1 (2)	C(7)S	0.7494 (27)	−0.0568 (18)	−0.4126 (20)	11. (1)
C(29)1	0.2057 (16)	0.9743 (09)	−0.1107 (10)	2.1 (2)	C(8)S	0.654 (03)	−0.0076 (20)	−0.3615 (18)	10. (2)
C(30)1	0.2486 (15)	0.9133 (09)	−0.1545 (09)	1.8 (2)	C(9)S	0.524 (03)	0.0295 (19)	−0.3853 (17)	5. (1)
C(31)1	0.2590 (15)	0.8208 (08)	−0.0939 (09)	1.6 (2)	C(10)S	0.4893 (23)	0.0171 (16)	−0.4597 (16)	6. (1)
C(32)1	0.2973 (14)	0.7390 (08)	−0.1146 (08)	1.3 (2)	H2S	0.234 (03)	0.0684 (25)	−0.5715 (27)	10.0
N(1)2	−0.0089 (12)	0.3811 (07)	0.1071 (07)	1.2 (2)	H3S	0.392 (04)	−0.0136 (24)	−0.6565 (20)	10.0
N(2)2	0.0635 (12)	0.2776 (07)	0.0241 (07)	1.3 (2)	H4S	0.610 (04)	−0.0759 (21)	−0.6177 (19)	10.0
N(3)2	0.0600 (11)	0.4376 (06)	−0.0880 (07)	1.0 (2)	H6S	0.7760 (26)	−0.1013 (20)	−0.5209 (24)	10.0
N(4)2	−0.0823 (12)	0.4308 (07)	0.2387 (07)	1.3 (2)	H7S	0.837 (03)	−0.0817 (22)	−0.3971 (25)	10.0
C(1)2	−0.0445 (14)	0.3660 (08)	0.2028 (08)	1.2 (2)	H8S	0.679 (04)	0.0003 (24)	−0.3121 (20)	10.0
C(2)2	−0.0335 (14)	0.2680 (08)	0.2600 (08)	1.3 (2)	H9S	0.460 (04)	0.0626 (23)	−0.3509 (20)	10.0
C(3)2	−0.0604 (16)	0.2189 (09)	0.3581 (09)	1.8 (2)	01	0.1039 (12)	0.8399 (07)	0.4127 (06)	4.8 (3)
C(4)2	−0.0452 (16)	0.1250 (09)	0.3902 (09)	1.8 (2)	02	0.1530 (13)	0.7362 (06)	0.3034 (08)	5.3 (3)
C(5)2	−0.0041 (16)	0.0817 (09)	0.3267 (10)	2.1 (2)	03	0.3727 (09)	0.8526 (09)	0.2782 (09)	9.9 (5)
C(6)2	0.0239 (15)	0.1286 (08)	0.2298 (09)	1.5 (2)	04	0.1279 (14)	0.9267 (07)	0.2195 (07)	6.6 (4)
C(7)2	0.0074 (14)	0.2237 (08)	0.1971 (08)	1.4 (2)					

both with 100 kHz field modulation as described previously.[16] For single crystal measurements at X-band frequencies crystals were mounted on a quartz rod that was attached to a goniometer and placed in the resonance cavity of the spectrometer. For single crystal measurements at Q-band frequencies the crystals were mounted on fixed quartz rods and the magnet was rotated. In both cases rotation angles were measured to a precision of ±1°. Variable-temperature measurements were accomplished with a nitrogen gas-flow system or by immersing the samples in liquid nitrogen or helium. Absolute spin susceptibility measurements were made at room temperature with the use of a powdered sample of $[Ni(tatbp)]_3[ReO_4]_2 \cdot C_{10}H_7Cl$. An identically prepared powdered sample of Ni(pc)I was used as a spin susceptibility standard because the spin susceptibility of Ni(pc)I is accurately known[16a] and its ESR properties are similar to those of $[Ni(tatbp)]_3[ReO_4]_2 \cdot C_{10}H_7Cl$.

Magnetic Susceptibility Measurements. Static magnetic susceptibility measurements were taken with a S.H.E. VTS-50 SQUID susceptometer. The sample holder was made of high purity Spectrosil quartz (Thermal American, Inc. NJ) and its background magnetic contribution was measured over the full temperature range just prior to measuring the sample. The sample magnetism was determined from the average of ten measurements taken at each temperature. The sample weights and applied fields used were 10 kG and 32.4 mg for $[Ni(tatbp)]_3[ReO_4]_2 \cdot C_{10}H_7Cl$ and 5 kG and 18.4 mg for $[Cu(tatbp)]_3[ReO_4]_2 \cdot C_{10}H_7Cl$.

Single-Crystal Electrical Conductivity Measurements. The electrical conductivity along the needle (*a*) axis of single crystals of $[Ni(tatbp)]_3[ReO_4]_2 \cdot C_{10}H_7Cl$ and $[Cu(tatbp)]_3[ReO_4]_2 \cdot C_{10}H_7Cl$ was measured with a four-probe ac (27 Hz) phase-locked technique described previously.[17] All electrical contacts were made with a conductive silver paint (Du Pont, conductor composition 4929). A sampling current of 1 μA was passed through the outer two contacts and the voltage drop was measured across the inner two contacts. The conductivity, $\sigma_\parallel$ (Ω^{-1} cm^{-1}), was calculated from the relation $\sigma_\parallel = L/(R_\parallel A)$, where L is the separation between the two inner contacts of the four probes, A is the cross-sectional area of the crystal, and $R_\parallel$ is the resistance. The dimensional parameters

(16) Phillips, T. E.; Scaringe, R. P.; Hoffman, B. M.; Ibers, J. A. *J. Am. Chem. Soc.* **1980**, *102*, 3435–3444.

(17) Phillips, T. E.; Anderson, J. R.; Schramm, C. J.; Hoffman, B. M. *Rev. Sci. Instrum.* **1979**, *50*, 236–265.

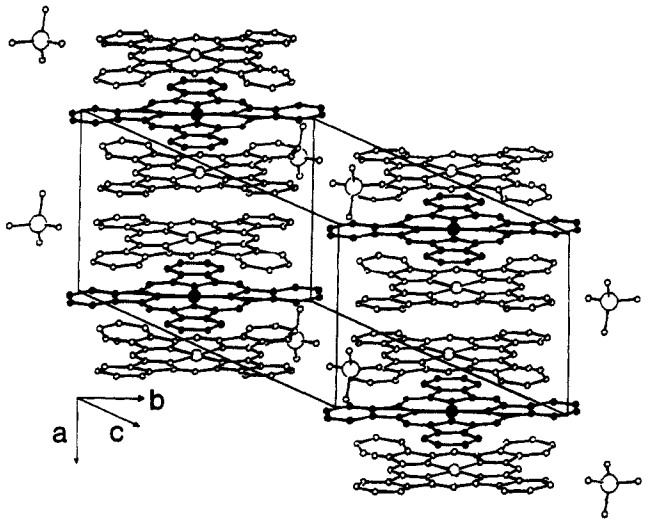

Figure 1. Crystal packing diagram of $[Cu(tatbp)]_3[ReO_4]_2 \cdot C_{10}H_7Cl$. Hydrogen atoms and solent molecules have been omitted for clarity. The central macrocycle of each trimer is darkened.

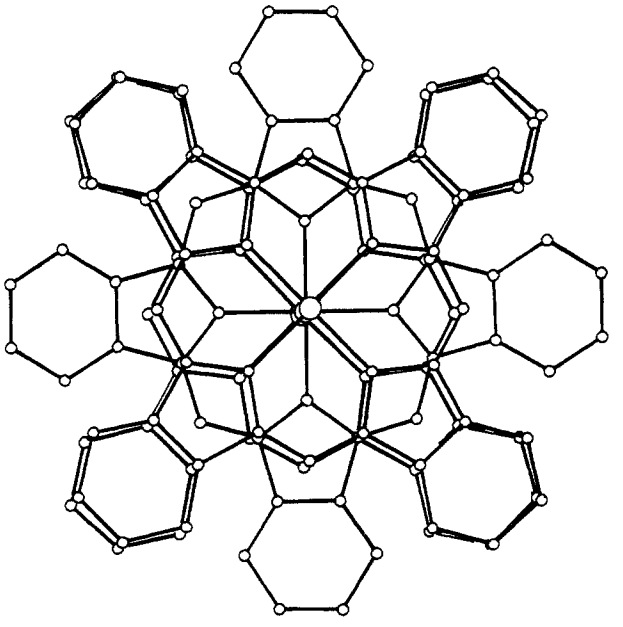

Figure 2. View perpendicular to the mean molecular planes of a Cu(tatbp) trimer.

L and *A* varied within the ranges of 0.05–0.015 cm and 5.1×10^{-4} to 1.7×10^{-5} cm^2, respectively. The uncertainties in the measurements of sample dimensions are estimated to cause an uncertainty in the absolute conductivity of 25%. These needle-shaped crystals are too thin to enable the measurement of conductivity perpendicular to the needle axis.

Results and Discussion

Description of Crystal Structure. $[Cu(tatbp)]_3[ReO_4]_2 \cdot C_{10}H_7Cl$ crystallizes in space group $P\bar{1}$ with three macrocycles in the cell. The partially (+2/3) ligand-oxidized metallomacrocycles are arranged in stacks. In channels between the stacks the ReO_4 anions and a disordered 1-chloronaphthalene solvent molecule reside. The crystal packing is illustrated in Figure 1. A single trimer is illustrated in Figure 2. This trimer consists of a centrosymmetric middle metallomacrocycle (Cu(2)) and an outer metallomacrocycle (Cu(1)) and its centrosymmetric pair. Both independent Cu(tatbp) units are essentially planar: the middle plane has an average deviation of 0.019 Å and a maximum deviation from the best least-squares plane of 0.045 Å; the outer unit shows greater deviation from planarity with an average deviation of 0.090 Å and a maximum deviation of 0.33 Å. In this outer unit the Cu(1) atom is displaced 0.039 (1) Å from the plane in a direction away from the middle plane while the peripheral

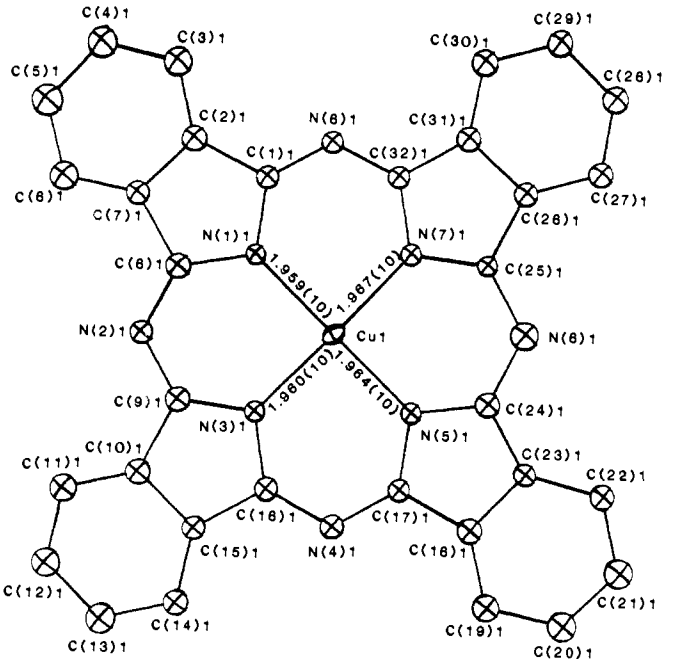

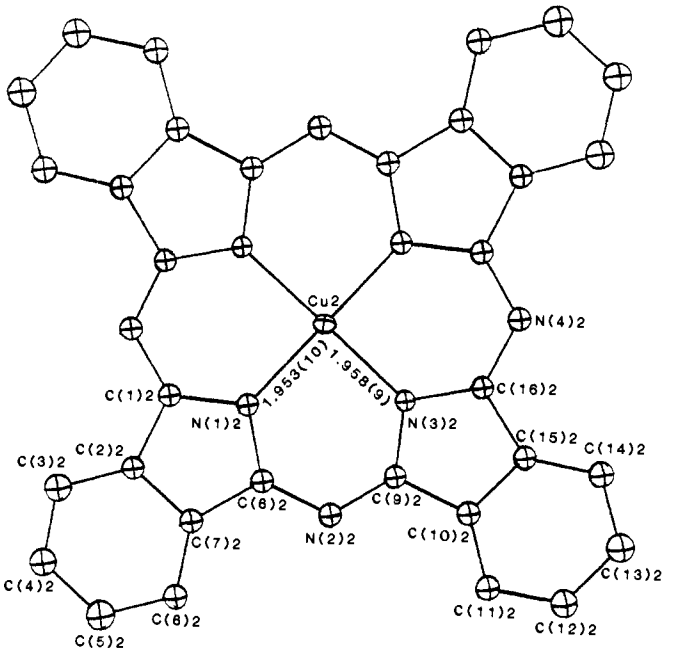

Figure 3. Labeling scheme for the two unique Cu(tatbp) cations in $[Cu(tatbp)]_3[ReO_4]_2 \cdot C_{10}H_7Cl$. Atoms N(2), N(4), N(6), and N(8) are taken to be 75% N and 25% C as described in the text.

atoms of this outer plane are displaced in the direction of the middle plane. The angle between the middle and outer planes is 0.6°. The middle plane is rotated 44.7° with respect to the outer plane and hence is almost ideally staggered with respect to that plane. The Cu(1)–Cu(2) distance is 3.190 (3) Å while atom Cu(1) is 3.188 Å from the middle plane; hence displacement of these planes is slight. The normal to the trimer unit makes an angle of 7.8° with the crystallographic needle axis (*a*). Details on these least-squares planes are given in Table V.[15]

Table VI summarizes intramolecular bond distances and angles for the cations and anion. The labeling scheme for the cations is shown in Figure 3. There are no significant deviations in metrical details between the present cations and the Cu(tatbp) cation in Cu(tatbp)I.[7a]

Single-Crystal Electrical Conductivity. The room-temperature conductivity measured along the needle (*a*) axis of crystals of $[Ni(tatbp)]_3[ReO_4]_2 \cdot C_{10}H_7Cl$ or $[Cu(tatbp)]_3[ReO_4]_2 \cdot C_{10}H_7Cl$ is the same, $\sigma \approx 2.5\text{–}3.0 \times 10^{-4}\ \Omega^{-1}\ cm^{-1}$. This value is seven orders

Table VI. Selected Bond Distances (Å) and Angles (deg) for $[Cu(tatbp)_3[ReO_4]_2 \cdot C_{10}H_7Cl$

bond	macrocycle 1 dist. or angle	av	bond	macrocycle 2 dist or angle	av
Cu–N(1)	1.959 (10)				
Cu–N(3)	1.960 (10)				
Cu–N(5)	1.964 (10)		Cu–N(1)	1.953 (10)	
Cu–N(7)	1.967 (10)	1.962 (10)[a]	Cu–N(3)	1.958 (9)	1.955 (10)
N(1)–C(1)	1.375 (14)				
N(1)–C(8)	1.374 (15)				
N(3)–C(9)	1.384 (15)				
N(3)–C(16)	1.382 (14)				
N(5)–C(17)	1.388 (14)		N(1)–C(1)	1.390 (14)	
N(5)–C(24)	1.380 (14)		N(1)–C(8)	1.387 (15)	
N(7)–C(25)	1.376 (15)		N(3)–C(9)	1.364 (14)	
N(7)–C(32)	1.376 (14)	1.379 (15)	N(3)–C(16)	1.360 (14)	1.377 (15)
N(2)–C(8)	1.345 (15)				
N(2)–C(9)	1.324 (15)				
N(4)–C(16)	1.311 (15)				
N(4)–C(17)	1.326 (15)				
N(6)–C(24)	1.374 (15)		N(2)–C(8)	1.332 (15)	
N(6)–C(25)	1.391 (16)		N(2)–C(9)	1.347 (15)	
N(8)–C(1)	1.332 (15)		N(4)–C(1)	1.342 (15)	
N(8)–C(32)	1.345 (15)	1.344 (28)	N(4)–C(16)	1.355 (15)	1.344 (15)
C(1)–C(2)	1.463 (16)				
C(7)–C(8)	1.454 (16)				
C(9)–C(10)	1.474 (16)				
C(15)–C(16)	1.467 (16)				
C(17)–C(18)	1.436 (16)		C(1)–C(2)	1.458 (15)	
C(23)–C(24)	1.447 (15)		C(7)–C(8)	1.456 (16)	
C(25)–C(26)	1.388 (16)		C(9)–C(10)	1.454 (16)	
C(31)–C(32)	1.451 (16)	1.447 (16)	C(15)–C(16)	1.450 (15)	1.454 (16)
C(2)–C(7)	1.371 (16)				
C(10)–C(15)	1.381 (16)				
C(18)–C(23)	1.398 (16)		C(2)–C(7)	1.393 (16)	
C(26)–C(31)	1.381 (16)	1.383 (16)	C(10)–C(15)	1.400 (16)	1.396 (16)
C(2)–C(3)	1.378 (17)				
C(6)–C(7)	1.398 (17)				
C(10)–C(11)	1.360 (17)				
C(14)–C(15)	1.390 (17)				
C(18)–C(19)	1.380 (17)		C(2)–C(3)	1.395 (17)	
C(22)–C(23)	1.398 (17)		C(6)–C(7)	1.388 (16)	
C(26)–C(27)	1.430 (16)		C(10)–C(11)	1.391 (16)	
C(30)–C(31)	1.403 (17)	1.393 (21)	C(14)–C(15)	1.375 (16)	1.387 (17)
C(3)–C(4)	1.395 (18)				
C(5)–C(6)	1.373 (18)				
C(11)–C(12)	1.399 (18)				
C(13)–C(14)	1.392 (18)				
C(19)–C(20)	1.381 (17)		C(3)–C(4)	1.370 (17)	
C(21)–C(22)	1.380 (17)		C(5)–C(6)	1.374 (17)	
C(27)–C(28)	1.386 (17)		C(11)–C(12)	1.390 (17)	
C(29)–C(30)	1.376 (18)	1.385 (18)	C(13)–C(14)	1.385 (17)	1.380 (17)
C(4)–C(5)	1.399 (18)				
C(12)–C(13)	1.394 (19)				
C(20)–C(21)	1.396 (17)		C(4)–C(5)	1.391 (18)	
C(28)–C(29)	1.394 (18)	1.396 (19)	C(12)–C(13)	1.393 (17)	1.392 (18)
N(1)–Cu–N(3)	89.7 (4)				
N(3)–Cu–N(5)	89.3 (4)				
N(5)–Cu–N(7)	90.8 (4)		N(1)–Cu–N(3)	89.8 (4)	
N(7)–Cu–N(1)	90.2 (4)	90.0 (6)	N(1)–Cu–N(3)′	90.2 (4)	90.0 (4)
Cu–N(1)–C(1)	126.3 (8)				
Cu–N(1)–C(8)	126.8 (8)				
Cu–N(3)–C(9)	126.0 (8)				
Cu–N(3)–C(16)	125.9 (8)				
Cu–N(5)–C(17)	126.5 (8)		Cu–N(1)–C(1)	126.7 (8)	
Cu–N(5)–C(24)	126.7 (8)		Cu–N(1)–C(8)	126.7 (8)	
Cu–N(7)–C(25)	128.2 (8)		Cu–N(3)–C(9)	126.0 (8)	
Cu–N(7)–C(32)	125.7 (8)	126.5 (8)	Cu–N(3)–C(16)	126.8 (8)	126.5 (8)
C(1)–N(1)–C(8)	107.0 (10)				
C(9)–N(3)–C(16)	108.0 (10)				
C(17)–N(5)–C(24)	106.7 (10)		C(1)–N(1)–C(8)	106.6 (10)	
C(25)–N(7)–C(32)	106.1 (10)	106.9 (10)	C(9)–N(3)–C(16)	107.2 (10)	106.9 (10)
C(8)–N(2)–C(9)	123.0 (11)				
C(16)–N(4)–C(17)	123.6 (11)				
C(24)–N(6)–C(25)	124.7 (10)		C(8)–N(2)–C(9)	121.9 (11)	
C(1)–N(8)–C(32)	122.7 (11)	123.5 (11)	C(16)–N(4)–C(1)	123.9 (10)	122.9 (15)

Table VI (Continued)

bond	macrocycle 1 dist. or angle	av	bond	macrocycle 2 dist or angle	av
N(1)-C(1)-N(8)	127.4 (11)				
N(1)-C(8)-N(2)	126.9 (11)				
N(2)-C(9)-N(3)	127.6 (11)				
N(3)-C(16)-N(4)	128.1 (11)				
N(4)-C(17)-N(5)	126.5 (11)		N(1)-C(1)-N(4)	126.0 (11)	
N(5)-C(24)-N(6)	125.6 (11)		N(1)-C(8)-N(2)	127.1 (11)	
N(6)-C(25)-N(7)	124.0 (11)		N(2)-C(9)-N(3)	128.5 (11)	
N(7)-C(32)-N(8)	127.7 (11)	126.7 (13)	N(3)-C(16)-N(4)	126.4 (11)	127.0 (11)
N(1)-C(1)-C(2)	109.7 (10)				
N(1)-C(8)-C(7)	110.0 (10)				
C(3)-C(9)-C(10)	109.6 (10)				
N(3)-C(16)-C(15)	108.5 (10)				
N(5)-C(17)-C(18)	110.1 (10)		N(1)-C(1)-C(2)	109.9 (10)	
N(5)-C(24)-C(23)	110.1 (10)		N(1)-C(8)-C(7)	110.3 (10)	
N(7)-C(25)-C(26)	111.3 (11)		N(3)-C(9)-C(10)	110.0 (10)	
N(7)-C(32)-C(31)	109.2 (10)	109.8 (11)	N(3)-C(16)-C(15)	110.9 (10)	110.3 (10)
N(8)-C(1)-C(2)	122.9 (11)				
N(2)-C(8)-C(7)	123.1 (11)				
N(2)-C(9)-C(10)	122.8 (11)				
N(4)-C(16)-C(15)	123.5 (11)				
N(4)-C(17)-C(18)	123.4 (11)		N(4)-C(1)-C(2)	124.2 (11)	
N(6)-C(24)-C(23)	124.3 (11)		N(2)-C(8)-C(7)	122.6 (11)	
N(6)-C(25)-C(26)	124.7 (11)		N(2)-C(9)-C(10)	121.4 (11)	
N(8)-C(32)-C(31)	123.1 (11)	123.5 (11)	N(4)-C(16)-C(15)	122.7 (11)	122.7 (11)
C(1)-C(2)-C(3)	131.6 (12)				
C(6)-C(7)-C(8)	130.9 (12)				
C(9)-C(10)-C(11)	131.1 (12)				
C(14)-C(15)-C(16)	130.5 (12)				
C(17)-C(18)-C(19)	131.0 (12)		C(1)-C(2)-C(3)	131.5 (11)	
C(22)-C(23)-C(24)	133.2 (11)		C(6)-C(7)-C(8)	132.4 (11)	
C(25)-C(26)-C(27)	133.2 (11)		C(9)-C(10)-C(11)	132.2 (11)	
C(30)-C(31)-C(32)	130.6 (12)	131.5 (12)	C(14)-C(15)-C(16)	133.3 (12)	132.3 (12)
C(1)-C(2)-C(7)	106.6 (11)				
C(2)-C(7)-C(8)	106.8 (11)				
C(9)-C(10)-C(15)	105.7 (11)				
C(10)-C(15)-C(16)	108.2 (11)				
C(17)-C(18)-C(23)	106.8 (11)		C(1)-C(2)-C(7)	106.8 (10)	
C(18)-C(23)-C(24)	106.3 (10)		C(2)-C(7)-C(8)	106.4 (10)	
C(25)-C(26)-C(31)	107.6 (11)		C(9)-C(10)-C(15)	106.6 (10)	
C(26)-C(31)-C(32)	105.9 (11)	106.7 (11)	C(10)-C(15)-C(16)	105.3 (10)	106.3 (10)
C(3)-C(2)-C(7)	121.7 (12)				
C(2)-C(7)-C(6)	122.2 (12)				
C(11)-C(10)-C(15)	123.1 (12)				
C(10)-C(15)-C(14)	121.1 (12)				
C(19)-C(18)-C(23)	122.2 (12)		C(3)-C(2)-C(7)	121.7 (11)	
C(18)-C(23)-C(22)	120.5 (11)		C(2)-C(7)-C(6)	121.2 (11)	
C(27)-C(26)-C(31)	119.2 (11)		C(11)-C(10)-C(15)	121.2 (11)	
C(26)-C(31)-C(30)	123.5 (12)	121.6 (14)	C(10)-C(15)-C(14)	121.4 (11)	121.4 (11)
C(2)-C(3)-C(4)	116.8 (12)				
C(5)-C(6)-C(7)	116.5 (12)				
C(10)-C(11)-C(12)	116.4 (12)				
C(13)-C(14)-C(15)	116.8 (12)				
C(18)-C(19)-C(20)	117.1 (12)		C(2)-C(3)-C(4)	117.0 (12)	
C(21)-C(22)-C(23)	117.1 (11)		C(5)-C(6)-C(7)	116.1 (11)	
C(26)-C(27)-C(28)	117.8 (11)		C(10)-C(11)-C(12)	116.8 (11)	
C(29)-C(30)-C(31)	115.7 (12)	116.8 (12)	C(13)-C(14)-C(15)	117.9 (12)	116.9 (12)
C(3)-C(4)-C(5)	121.2 (13)				
C(4)-C(5)-C(6)	121.6 (13)				
C(11)-C(12)-C(13)	121.6 (13)				
C(12)-C(13)-C(14)	120.9 (13)				
C(19)-C(20)-C(21)	121.4 (12)		C(3)-C(4)-C(5)	120.7 (12)	
C(20)-C(21)-C(22)	121.7 (12)		C(4)-C(5)-C(6)	121.4 (12)	
C(27)-C(28)-C(29)	120.5 (13)		C(11)-C(12)-C(13)	121.9 (12)	
C(28)-C(29)-C(30)	123.3 (13)	121.5 (13)	C(12)-C(13)-C(14)	120.8 (12)	121.2 (12)
Re-O(1)	1.665 (11)				
Re-O(2)	1.673 (7)				
Re-O(3)	1.736 (9)				
Re-O(4)	1.730 (9)	1.697 (11)			
O(1)-Re-O(2)	112.5 (3)				
O(1)-Re-O(3)	109.5 (7)				
O(1)-Re-O(4)	109.8 (4)				
O(2)-Re-O(3)	109.1 (7)				
O(2)-Re-O(4)	109.4 (5)				
O(3)-Re-O(4)	106.3 (6)	110.2 (19)			

[a] The standard deviation of a single observation is given in parentheses. It is the larger of that estimaed for a single observation from the inverse matrix or on the assumption that the values averaged are from the same population.

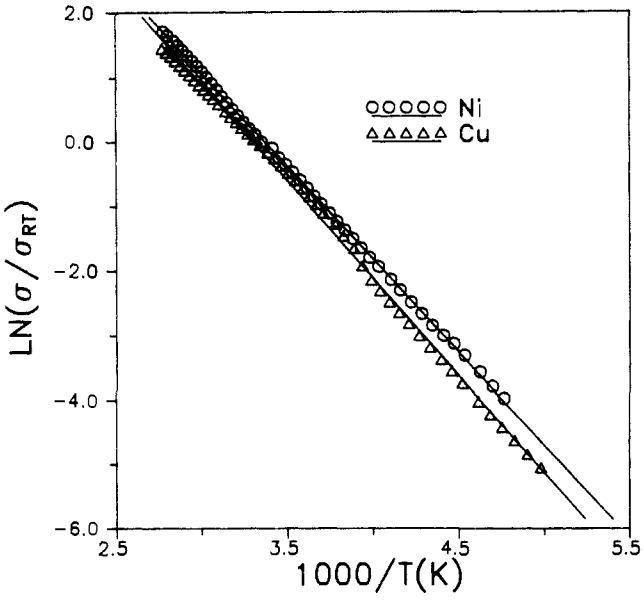

Figure 4. Temperature dependence of the normalized conductivity.

of magnitude less than that of the most highly conducting M(L)I compounds and is comparable to the values for intrinsic atomic semiconductors, such as silicon. The crystals are semiconductors, $\sigma(T)$ increasing exponentially as the temperature is increased. Plots of ln $(\sigma(T)/\sigma(RT))$ vs $1000/T$ (Figure 4) for typical crystals of $[Ni(tatbp)]_3[ReO_4]_2 \cdot C_{10}H_7Cl$ and $[Cu(tatbp)]_3[ReO_4]_2 \cdot C_{10}H_7Cl$ are linear, with slopes corresponding to activation energies for conduction in the range of 0.24–0.26 eV.

The semiconducting behavior can be rationalized when the trimeric nature of the conducting stacks is considered. Two electrons must be removed from every three metallomacrocycles to account for the stoichiometry; we show below that these electrons are removed from the p-π HOMOs of the tatbp ligand. Interaction of these ligand-based orbitals within a regular stack of partially oxidized M(L) molecules would give a $^2/_3$ filled conduction band; trimerization of the stacks, as in this material, opens gaps in this conduction band at $^1/_3$ filling and at $^2/_3$ filling, the Fermi level.[18] This latter gap renders the compound a semiconductor, as is frequently seen in a variety of salts of 7,7,8,8-tetracyanoquinodimethane (TCNQ).[19]

An alternative, but equivalent, view of the band structure of these materials can be developed by considering the individual trimers as supermolecules, with weak interactions between adjacent trimers (Figure 5). Interestingly, NMR studies[10] of solutions containing both oxidized and unoxidized M(L) species indicate that $[M(L)]_3^{2+}$ trimers also occur in solutions prepared with a ratio of $[M(L)]^0/[M(L)]^+ = 1/2$. As mentioned above, there are minimal distortions of the metal-over-metal stacking motif within a trimer, whereas adjacent trimers have appreciably slipped with respect to one another. Therefore, the transfer integral between orbitals within a trimer, t_{ra}, should be nearly identical with that of ~0.2 eV found in compounds with a regular metal-over-metal stacking structure, such as Ni(pc)I.[1c] Because of the more drastic dislocation of adjacent trimers the intertrimer transfer integral, t_{er}, should be relatively small, $t_{er} \ll t_{ra}$. The individual trimers can then be thought of as supermolecules that interact with each other weakly.[20] The p-π HOMOs of the three macrocycles within a trimer would then combine to form a

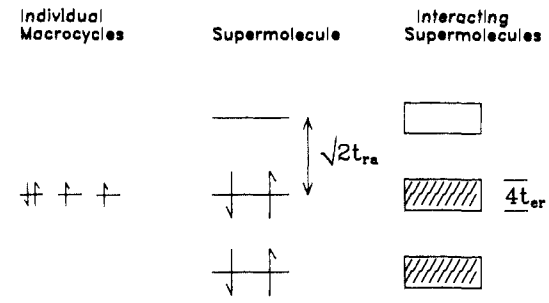

Figure 5. Sketch of the HOMOs of each macrocycle and their interaction to form trimer bands.

bonding, nonbonding, and antibonding orbital set for the supermolecule, with energy separations of $2^{1/2}t_{ra}$. When such supermolecules interact weakly to form an extended array, each of the three trimer orbitals would broaden into a band (Figure 5). For the 2/3 oxidized stacks that occur here the bonding and nonbonding orbitals of a trimer and bands of the stack would be filled and the band-gap for a semiconducting excitation to the antibonding band would be $\Delta = 2^{1/2}t_{ra} - 4t_{er}$. This view of a regular stack of weakly interacting trimers has the same consequence as the previous description in terms of distortions away from a regular lattice but will be useful in considering details of the Cu–Cu spin exchange in the $[Cu(tatbp)]_3[ReO_4]_2 \cdot C_{10}H_7Cl$ system.

Bulk Susceptibility Measurements on the Ni Salt. The measured room temperature static susceptibility of a powdered sample of $[Ni(tatbp)]_3[ReO_4]_2 \cdot C_{10}H_7Cl$ is $\chi = -9.49 \times 10^{-4}$ emu/mol. When corrected for core diamagnetism ($\chi^d = -1.12 \times 10^{-3}$ emu/mol)[21] the paramagnetic susceptibility is $\chi^p = 1.73 \times 10^{-4}$ emu/mol or 0.58×10^{-4} emu/(mol Ni(tatbp)) versus 1.11×10^{-4} emu/mol for Ni(pc)I.[1a] The temperature dependence of χ^p from 2 to 300 K follows the expression

$$\chi^p = C/T + Z \qquad (1)$$

where C is the Curie constant and Z is a temperature-independent contribution to the susceptibility. A least-squares fit of the data to eq 1 yields the values $C = 1.80 \times 10^{-2}$ emu mol^{-1} K^{-1} and $Z = 1.14 \times 10^{-4}$ emu/mol; within the accuracy of background and diamagnetic corrections this value of Z is not considered to be significantly different from zero.

The Curie constant can be interpreted from the relation

$$C = S(S+1)\left(\frac{Ng^2\beta^2}{3k_B}\right) \qquad (2)$$

where β is the Bohr magneton, k_B is Boltzmann's constant, S is the spin, g^2 is the average square of the spectroscopic splitting factor, and N is the number of localized non-interacting spin sites per mole. The measured Curie constant then corresponds to $N = 0.048$, or 0.016 g = 2.00 spins per Ni(tatbp) molecule. This level of localized, non-interacting spins can be assigned to impurities or lattice defect sites. Thus, this compound displays the essentially diamagnetic ground state expected for a simple semiconductor that contains low concentrations of paramagnetic impurities or lattice defect sites. This is consistent with the conductivity data and the picture of the band structure developed above.

Electron Spin Resonance Measurements of the Ni Salt. Information on the nature of the paramagnetic sites in $[Ni(tatbp)]_3[ReO_4]_2 \cdot C_{10}H_7Cl$ can be gained from ESR measurements. The room temperature spin susceptibility data for $[Ni(tatbp)]_3[ReO_4]_2 \cdot C_{10}H_7Cl$ indicate that the ESR signal intensity accounts

(18) Whangbo, M.-H. *Acc. Chem. Res.* **1983**, *16*, 95–101.
(19) Soos, Z. G.; Bondeson, S. R. In *Extended Linear Chain Compounds*; Miller, J. S., Ed.; Plenum Press: New York, 1983; Vol. 3, p 199.
(20) This approach has previously been used to explain the π-electron pairing in dimers formed in solutions of zinc and copper porphyrin π-cation radicals. (a) Fuhrhop, J. H.; Wasser, P.; Mauzerall, D. *J. Am. Chem. Soc.* **1972**, *94*, 7996–8001. (b) Cowan, J. A. *J. Chem. Soc., Dalton Trans.* **1988**, 2681–2682.
(21) From Pascals constants, see: (a) Drago, R. S. *Physical Methods in Chemistry*; W. B. Saunders: Philadelphia, PA, 1977; p 413. (b) Mulay, L. N.; Bourdreaux, E. A., Eds. *Theory and Applications of Molecular Diamagnetism*; Wiley: New York, 1976; p 307.

for 0.021 g = 2.00 spins per Ni(tatbp) molecule. This value is in good agreement with the Curie component of the bulk susceptibility. The temperature dependence of the ESR signal intensity for samples of $[Ni(tatbp)]_3[ReO_4]_2 \cdot C_{10}H_7Cl$ also is Curie-like; this is further evidence that the ESR signal arises from the same spins as the Curie component of the bulk susceptibility. Therefore information on these impurity spins may be derived from their ESR properties.

Single-crystal ESR studies reveal that crystals of $[Ni(tatbp)]_3[ReO_4]_2 \cdot C_{10}H_7Cl$ exhibit a single resonance with a temperature-independent axial **g** tensor whose unique axis corresponds to the normal to the M(L) planes, which can be taken as lying along the needle (*a*) axis.[22] The angular dependence of the *g* value can be fit to the equation

$$g(\phi) = [g_\parallel^2 \cos^2 \phi + g_\perp^2 \sin^2 \phi]^{1/2} \quad (3)$$

where ϕ is the angle between the needle axis and the applied magnetic field, leading to the values of $g_\parallel = 2.0028$ (4) and $g_\perp = 1.9996$ (4). The line width is also axial with the needle (*a*) axis approximating the unique axis and ranges from 7.4 G at $g_\parallel$ to 3.6 G at $g_\perp$. The angular dependence of the line width can be fit precisely to the equation

$$\Gamma(\phi) = \Gamma_0 + \Gamma_1(1 + \cos^2 \phi) \quad (4)$$

where the fit yields $\Gamma_0 = 1.37$ G and $\Gamma_1 = 3.65$ G.

The *g* value and line width of the ESR signal are typical of π-cation metallomacrocycle radicals.[23] The fact that the *g* value and line width tensors follow the crystal morphology indicates that the sites that give rise to the signal are oriented within the crystal in the same manner as the macrocycles. We interpret this to mean that the ESR signal and the Curie component of the bulk susceptibility arise from π-cation radical defect sites oriented within a chain, for example, chain breaks that result in incomplete trimers.

Bulk Susceptibility Measurements on the Cu Salt. The room temperature bulk susceptibility of a powdered sample of $[Cu(tatbp)]_3[ReO_4]_2 \cdot C_{10}H_7Cl$ is $\chi = 2.95 \times 10^{-3}$ emu/mol. When corrected for core diamagnetism ($\chi^d = -1.12 \times 10^{-3}$ emu/mol)[21] the paramagnetic susceptibility is $\chi^p = 4.07 \times 10^{-3}$ emu/mol. The temperature dependence of χ^p is plotted in Figure 6. The data follow the Curie–Weiss law

$$\chi^p = C/(T - \Theta) \quad (5)$$

as the temperature is lowered to 5 K. A least-squares fit of the data yields the constant $C = 1.19$ (2) emu mol^{-1} K^{-1}, in close agreement with that calculated from eq 2 for one Cu(II) spin per macrocycle with $g^2 = 4.332 = (2g_\perp^2 + g_\parallel^2)/3$: $C = 1.195$ emu mol^{-1} K^{-1}. The fit also gives a Weiss constant $\Theta = -5.2$ (3) K, indicative of strong antiferromagnetic Cu–Cu coupling within the one-dimensional chains. The deviation from the simple Curie law caused by a non-zero Θ is readily apparent in a plot of the temperature dependence of the quantity χ^pT (Figure 6, inset). At temperatures below 5 K χ^p increases more slowly than predicted by the fit. Antiferromagnetic deviations from high-temperature fits to eq 5 have been noted for other Cu macrocycle conductors.[6,7]

The Weiss constant for $[Cu(tatbp)]_3[ReO_4]_2 \cdot C_{10}H_7Cl$ is almost the same as those for Cu(pc)I, $\Theta = -4.18$ (3) K, or Cu(tatbp)I, $\Theta = -6.9$ (3) K. However, the iodinated materials behave as simple quasi one-dimensional metals and the strong Cu–Cu coupling indicated by these values was attributed to long-range spin exchange between Cu sites mediated by the metallic carriers

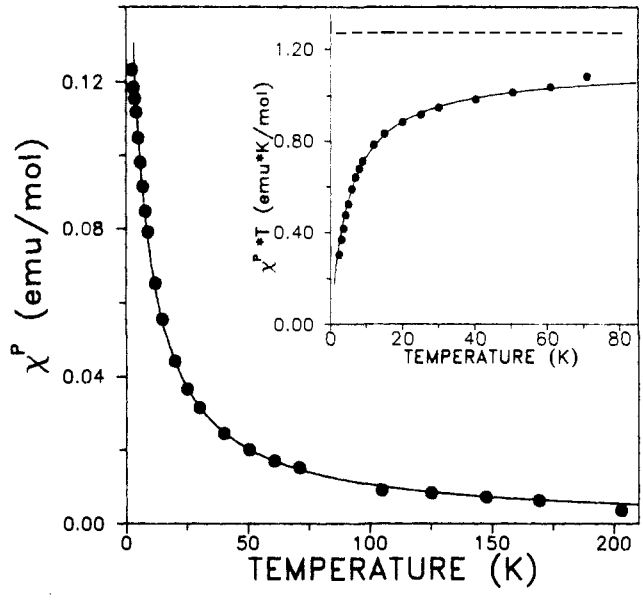

Figure 6. Temperature dependence of the paramagnetic susceptibility of $[Cu(tatbp)]_3[ReO_4]_2 \cdot C_{10}H_7Cl$. The inset shows the temperature dependence of the product χ^pT. The solid lines show the theoretical fit. The dashed line in the inset indicates the behavior expected for a system with the same Curie constant but a Weiss constant of zero.

(RKKY coupling), with average exchange coupling $J = k_B\Theta$.[6,7] This interpretation was based on NMR results for the Cu(pc)I system that indicate the direct exchange between spins in the Cu d-orbitals is small, $J_{dd}/k_B \leq 0.3$ K.[6b] In contrast, $[Cu(tatbp)]_3[ReO_4]_2 \cdot C_{10}H_7Cl$ is a semiconductor, not a metal, and there is no reason to expect that direct exchange is larger in $[Cu(tatbp)]_3[ReO_4]_2 \cdot C_{10}H_7Cl$ than in the iodinated materials because the Cu–Cu spacing is similar. Thus, the large, negative Weiss constant for the $[Cu(tatbp)]_3[ReO_4]_2 \cdot C_{10}H_7Cl$ system at first appears anomalous. However, we can understand it in terms of the band structure in which the π-HOMOs of the M(tatbp) within individual trimers strongly interact to form supermolecular orbitals (Figure 5). Spin polarization of the nonbonding band by intramolecular d-π exchange can mediate intermolecular Cu–Cu spin exchange within a trimer in much the same way that bonding electrons mediate the contact spin–spin coupling commonly observed in NMR experiments,[24] and the resulting Cu–Cu coupling constant, J_{ra}, should be of the same magnitude as that found in the molecular metals with undistorted stacks (J). In contrast, coupling between copper sites in adjacent trimers is expected to be small, $J_{er} \ll J_{ra}$.

The experimental Weiss constant derived from high-temperature susceptibility measurements corresponds to the root-mean-square average exchange coupling along a chain, J_{rms}: For the trimerized stacks, there are three unique couplings along the chain, two intratrimer and one intertrimer, and thus

$$\Theta/k_B = J_{rms} = \left(\frac{2J_{ra}^2 + J_{er}^2}{3}\right)^{1/2} \approx \left(\frac{2}{3}J_{ra}^2\right)^{1/2} \approx \left(\frac{2}{3}\right)^{1/2} J \quad (6)$$

Clearly, $[Cu(tatbp)]_3[ReO_4]_2 \cdot C_{10}H_7Cl$ and the Cu(L)I molecular metals have similar values of Θ because J_{rms} is dominated by intratrimer coupling similar to that in the regular stacks. This analysis is consistent with the view that Cu–Cu coupling along the distorted M(L) stacks in this compound as well as in the regular stacks of the Cu(L)I conductors is mediated by delocalized

(22) In principle the analysis should incorporate the slight deviation (7.8°) between the normal to the M(L) planes and the *a* axis. However, the precision of these measurements does not warrant this.

(23) Fajer, J.; Davis, S. M. In *The Porphyrins*; Dolphin, D., Ed.; Academic Press: New York, 1979; Vol. 4, pp 198–256.

(24) Carrington, A.; Mclachlan, A. D. *Introduction to Magnetic Resonance*; Harper & Row: New York, NY, 1967; pp 64–66.

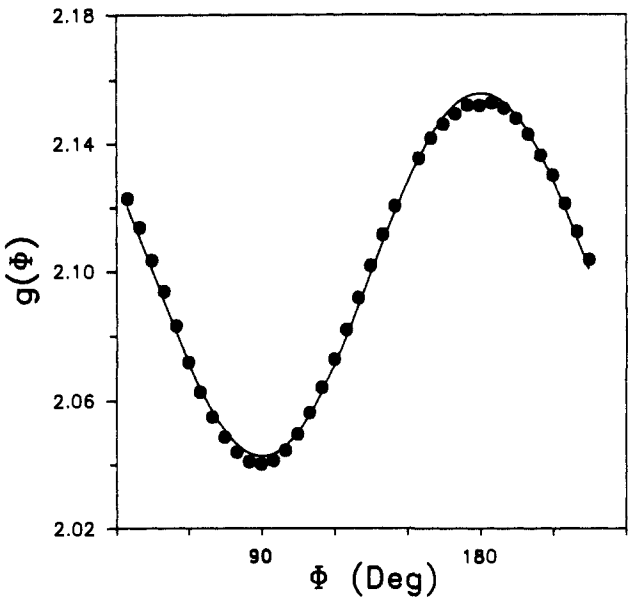

Figure 7. The angular dependence of the g value for $[Cu(tatbp)]_3[ReO_4]_2 \cdot C_{10}H_7Cl$. At $\phi = 180°$ the a axis is parallel to the applied field. The solid line is the theoretical fit.

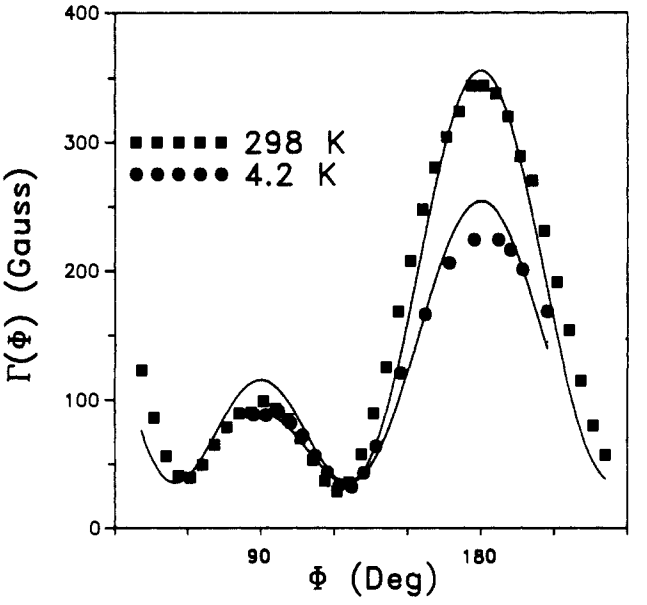

Figure 8. The angular dependence of the ESR line width for $[Cu(tatbp)]_3[ReO_4]_2 \cdot C_{10}H_7Cl$. At $\phi = 180°$ the a axis is parallel to the applied field. The solid lines are the theoretical fits.

π-electrons of the M(L) macrocycle.

Electron Spin Resonance Measurements on the Cu Salt. $[Cu(tatbp)]_3[ReO_4]_2 \cdot C_{10}H_7Cl$ has a single ESR signal with an axial **g** tensor typical of a copper porphyrin.[25] As for the Ni salt the normal to the macrocycle planes is the unique axis and can be taken as lying along the needle (a) axis.[22] The angular dependence of the g value for a single crystal can be fit precisely to eq 3 to yield the values $g_\parallel = 2.156$ (1) and $g_\perp = 2.043$ (1) (Figure 7). These g values of $[Cu(tatbp)]_3[ReO_4]_2 \cdot C_{10}H_7Cl$ are temperature independent, in sharp contrast to those for the Cu(L)I molecular metals where temperature-dependent g values indicative of strong spin exchange between the Cu(II) sites and the π-carrier electrons are observed.

ESR spectra of $[Cu(tatbp)]_3[ReO_4]_2 \cdot C_{10}H_7Cl$ powders show a striking resemblance to spectra obtained with solution samples containing $[Cu(OEP)]^+$ and Cu(OEP)[26] in a mole ratio of approximately 2:1.[10] In that case partial reduction of a solution of $[Cu(OEP)]^+$ π-cation radical did not result in spectra that were a simple summation of the individual spectra of $[Cu(OEP)]^+$ and Cu(OEP). One explanation proposed was that the signal arises from aggregates with spin-paired π-electrons but unpaired Cu(II) moments, similar to the trimeric supermolecules that comprise the M(L) stacks here.

The ESR line width of $[Cu(tatbp)]_3[ReO_4]_2 \cdot C_{10}H_7Cl$ is 345 G at $g_\parallel$ and 99 G at $g_\perp$ at room temperature, and its angular dependence can be fit to the equation

$$\Gamma(\phi) = \Gamma_1(3\cos^2\phi - 1)^2 + \Gamma_0 \quad (7)$$

with dipolar component, $\Gamma_1 = 80$ G, and isotropic component, $\Gamma_0 = 35$ G (Figure 8); results are identical in measurements at X-band (9.5 GHz) or Q-band (35 GHz).

A general equation that describes the angular dependence of the dipolar component of the ESR line width for systems of Heisenberg-exchange-coupled point dipoles of the type presented here is[27]

$$\Gamma(\phi) = A(3\cos^2\phi - 1)^2 + 10B(\sin\phi\cos\phi)^2 + C(\sin^4\phi) \quad (8)$$

This equation will reduce to the functional form of eq 7 under two sets of circumstances.[27] First, this will occur in the weak exchange limit where the exchange-frequency $\omega_e = J/h$ for coupling between adjacent dipoles is considerably smaller than the Larmor frequency, $\omega_e \ll \omega_0$. Second, if the exchange frequency between adjacent dipoles along a chain is large ($\omega_e > \omega_0$) but the coupling between chains is weak, then the exchange is one-dimensional and one finds $A \gg B, C$.

Weak exchange can be ruled out for $[Cu(tatbp)]_3[ReO_4]_2 \cdot C_{10}H_7Cl$ for this would require the bulk susceptibility to exhibit a Weiss constant $|\Theta| < h\omega_0/k \approx 0.5$ K, rather than the observed value of 5.2 K. Moreover, if one assumes $\omega_e \ll \omega_0$ and uses standard equations that express the dipolar line width, $\Gamma_1 = 80$ G, in terms of the known Cu–Cu distances and ω_e,[27] then one calculates $\omega_e = 2.4 \times 10^{11}$ s^{-1} which is greater than ω_0(X-band) $= 6 \times 10^{10}$ s^{-1}. Instead, the second set of circumstances must apply and the angular dependence of Γ may be accounted for by assuming strong Cu–Cu coupling in one direction only, J(intrachain) $\gg J$(interchain), consistent with the crystal structure in which the Cu chains are separated by ~16 Å. Systems with one-dimensional spin exchange can exhibit a one-dimensional ESR line shape, where deviation from a simple Lorentzian line shape is most pronounced at $g_\parallel$.[28] Unfortunately, the $g_\parallel$ line width for $[Cu(tatbp)]_3[ReO_4]_2 \cdot C_{10}H_7Cl$ is too broad to enable us to describe the line shape.

When crystals of $[Cu(tatbp)]_3[ReO_4]_2 \cdot C_{10}H_7Cl$ are cooled the angular dependence of the line width remains the same (Figure 8) and the widths decrease only moderately; at $T = 4.2$ K $\Gamma_1 = 56$ G and $\Gamma_0 = 35$ G; the slight narrowing upon cooling may well reflect an increase in J_{rms} caused by thermal contraction of the crystals. This weak temperature dependence is in sharp contrast with the behavior of the Cu(L)I systems where metallic charge carriers mediate strong spin exchange within the Cu chains; for these highly conductive crystals, the line width increases strongly at low temperatures.

Magnetic Data for $[Ni_{1-x}Cu_x(tatbp)]_3[ReO_4]_2 \cdot C_{10}H_7Cl$. When the electrocrystallization procedure is applied to starting materials that include one part Cu(tatbp) to six parts Ni(tatbp) the resulting crystals are a solid solution of the M = Ni and Cu materials. The ESR spectrum of a powdered sample of this compound with $x = 0.28$ shown in Figure 9 appears to include a contribution from isolated Cu(L) that gives partially resolved copper and nitrogen hyperfine structure. In contrast, resolved hyperfine structure is never observed in $Ni_{1-x}Cu_x$(pc)I alloys of any composition owing to coupling of the copper(II) local moments and the conduction electrons in these molecular metals.[7] The resolved hyperfine

(25) Lin, W. C. In *The Porphyrins*; Dolphin, D., Ed.; Academic Press: New York, 1979; Vol. 4, pp 355–364.
(26) OEP = 2,3,7,8,12,13,17,18-octaethylporphyrinato dianion.
(27) McGregor, K. T.; Soos, Z. G. *J. Chem. Phys.* **1976**, *64*, 2506–2517.
(28) Hennessy, M. J.; McElwee, C. D.; Richards, P. M. *Phys. Rev. B* **1973**, *7*, 930–947.

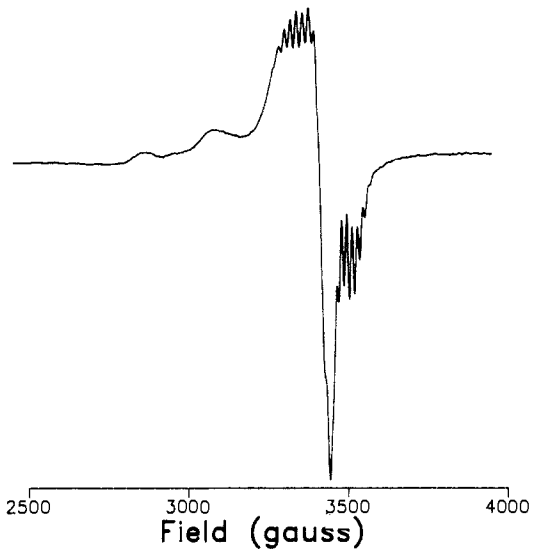

Figure 9. The ESR spectrum of a powdered sample of a $[Ni_{1-x}Cu_x(tatbp)]_3[ReO_4]_2 \cdot C_{10}H_7Cl$ solid solution. In this material 28% of the metal sites are occupied by Cu(II) ions.

structure likely is associated with trimers of the type [Ni(tatbp)-Cu(tatbp)-Ni(tatbp)]$^{2+}$. Observation of such structure is clear evidence that Cu-Cu spin exchange mediated by polarization of electrons in the nonbonding band of this semiconductor is not long range. In turn, this is consistent with the picture of strong Cu-Cu interactions within trimers but weak interactions between copper sites in different trimers.

Conclusions

$[Ni(tatbp)]_3[ReO_4]_2 \cdot C_{10}H_7Cl$ is a ligand-oxidized semiconductor with a band structure that can be derived by viewing the crystal packing as an extended array of weakly interacting supermolecules, each of which is composed of a trimer of three metallomacrocycles. The isostructural $[Cu(tatbp)]_3[ReO_4]_2 \cdot C_{10}H_7Cl$ exhibits strong Cu-Cu exchange coupling similar to that observed in Cu(L)I metallic conductors, and like the Cu(L)I metals this coupling is mediated by the π-electrons in the ligand-based band structure. However, metallic carrier electrons in the Cu(L)I systems move freely throughout the crystal lattice and mediate long-range Cu-Cu coupling, whereas ESR data on a $[Ni_{1-x}Cu_x(tatbp)]_3[ReO_4]_2 \cdot C_{10}H_7Cl$ solid solution indicate that the Cu-Cu coupling in this semiconductor is primarily limited to a trimer.

Acknowledgment. This work was supported by the National Science Foundation through Grant DMR-8818599 (B.M.H.) and through the Northwestern University Materials Research Center, Grant DMR-8821571.

Supplementary Material Available: Tables of anisotropic thermal parameters for Re and Cu and least-squares planes (2 pages); listing of $10|F_o|$ vs $10|F_c|$ (21 pages). Ordering information is given on any current masthead page.

Origin of the Strong Binding of Adenine to a Molecular Tweezer

James F. Blake and William L. Jorgensen*

Contribution from the Department of Chemistry, Purdue University, West Lafayette, Indiana 47907. *Received March 7, 1990*

Abstract: Monte Carlo statistical mechanics simulations and analyses of intrinsic interaction energies have been used to elucidate the observed strong binding of adenine derivatives to Zimmerman's molecular tweezer **3** in chloroform. Hydrogen bonding and π-stacking are found to contribute about equally to the remarkably strong interaction of the acid tweezer **6** and 9-methyladenine. The binding in chloroform is not enhanced by the existence of a naked binding cleft. Though 9-methyladenine easily wins the competition with chloroform for the binding site in **6**, the interaction between the ester tweezer **7** and 9-methyladenine is not adequate to displace the one or two chloroform molecules in the cleft. The absolute free energy of binding for the acid **6** and 9-methyladenine in chloroform was computed with the double-annihilation technique. The accord with the experimental data for acid **3** provides support for the validity of the theoretical analyses.

Specific interactions with nucleotide bases are under scrutiny in diverse areas including ribozyme chemistry,[1] formation of triple-helical DNA,[2] drug-DNA binding,[3] the chemistry of nucleic acid binding proteins,[4] and the association of chromosomes.[5] Much related activity is focusing on the development of synthetic hosts for the nucleoside bases. These studies are yielding valuable information on the factors that control molecular recognition in addition to providing a basis for the creation of novel, sequence-specific agents.[6] In fact, synthetic receptors have now been reported for all of the nucleoside bases.[7-10] Binding has been observed in chloroform solutions and features multiple hydrogen-bonding contacts and, sometimes, π-stacking interactions.

Hosts for adenine have been reported the most; it is an attractive target in view of the possibilities for both Watson-Crick and Hoogsteen hydrogen bonding. This is illustrated in Chart I where

Chart I

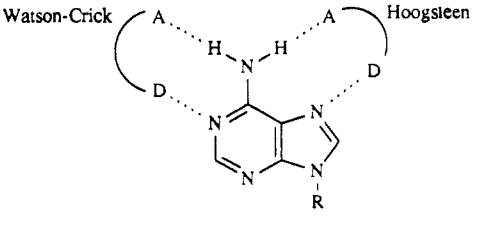

D and A refer to hydrogen-bond donor and acceptor sites. Elegant diversity is reflected in the structures of the adenine hosts, **1-4**,

* Address correspondence to this author at the Department of Chemistry, Yale University, New Haven, CT 06511.

(1) (a) Cech, T. R. *Science* **1987**, *236*, 1532. (b) Altman, S. *Adv. Enzymol.* **1989**, *62*, 1. (c) Piccirilli, J. A.; Krauch, T.; Moroney, S. E.; Benner, S. A. *Nature* **1990**, *343*, 33.

(2) (a) Moser, H. E.; Dervan, P. *Science* **1987**, *238*, 645. (b) Felsenfeld, G.; Davies, D. R.; Rich, A. *J. Am. Chem. Soc.* **1957**, *79*, 2023.

0002-7863/90/1512-7269$02.50/0 © 1990 American Chemical Society